Bimaterial Interfacial Crack Growth With Strain Gradient Theory

Su Hao
Research Scientist.
e-mail: suhao@tam3.mech.nwu.edu

Wing Kam Liu
Professor of Mechanical and Civil Engineering.
Fellow ASME
e-mail: w-liu@nwu.edu

Department of Mechanical Engineering,
Northwestern University,
2145 Sheridan Road,
Evanston, IL 60208

The purpose of this paper is to investigate the effect of material heterogeneity on damage evolution and subsequent crack propagation in bimaterial systems. Strain gradient theory analysis reveals that a higher stress triaxiality always occurs on the softer material side due to the material mismatch in yield capacity and the corresponding strain gradient along the interface. High stress triaxiality is a major condition which promotes ductile damage and facilitates crack growth. To investigate this link, numerical simulations of ductile interface crack growth are performed using a damage based constitutive model. Both the numerical and experimental results show that a crack may grow along the interface or deviate into the softer material, but never turn into the harder material. The theoretical and numerical analysis reveal three factors which strongly affect the direction of crack growth and the resistance capacity of the bimaterial system against fracture. These are the boundary conditions which determine the global kinematically admissible displacement field, the stress/strain gradient near the interface due to the material mismatch, and the distance from the crack tip to the interface.

1 Introduction

Experimental observations reveal that the fracture behavior of an interfacial crack in a bimaterial system differs from that of the homogeneous case. Figures 1 and 2, taken from reference by (Hao et al., 1996), show two extreme cases where the bonded materials differ in yield strength and hardening properties. In Fig. 1, the processes of micro-void nucleation, growth and coalescence result in crack growth along the interface in a TPB specimen, whereas in Fig. 2 the crack in a CCP specimen grows away from the interface and into the softer material. Crack growth is determined by material toughness, crack geometry, and the boundary conditions; and it is also directly relevant to the capacity of the structure to resist fracture and failure. The fracture toughness of a bimaterial specimen is usually lower than that of the homogeneous specimen subjected to similar boundary conditions. This decrease is strongly dependent on the crack growth path. For instance, the fracture toughness for crack growth along an interface (Fig. 1) is much different than crack growth along a shear band (Fig. 2).

Material heterogeneity and material compounds with a mismatch in mechanical properties are frequently found in many applications. The following questions are therefore of vital interest to both theoretical analysis and application:

- What is the effect of the material mismatch on crack growth behavior in a bimaterial system?
- What is the relationship between a growing interface crack path and the fracture toughness of the system?

In the past decade considerable effort has been concentrated on the interface crack problem via experimental investigation (I. E. Reimanis, 1990; Evans and Dalgleish, 1990; Petrovski and Kocak, 1993), numerical simulation (Shih and Asaro, 1991; Zywicz and Parks, 1992; Xu and Needleman, 1995), and theoretical analysis (Williams, 1959; Hutchinson et al., 1987; Rice, 1988). From the experimental research for homogeneous materials it is well known that crack growth, especially in a ductile material, is the accumulation of localized large plastic strain and damage in the form of voids, micro-cracks, or other kinds of micro-defects. An increasing amount of experimental observation demonstrate that the evolution of this damage, e.g., the void nucleation that is debonding the interface, starts at a very small length scale (less than 1 μm). Under such a small length scale, materials display strong size effects when a non-uniform plastic deformation takes place. These size effects are especially strong in a bimaterial system since the material mismatch usually causes a highly localized strain gradient near the interface (Fleck and Hutchinson, 1993). It can be anticipated that this gradient will be extremely high if a crack tip is located close to the interface, as illustrated in Fig. 3.

To analyze interface cracking phenomena the strain gradient theory has been developed (Fleck and Hutchinson, 1993; Fleck and Hutchinson, 1997). Based on a multi-scale framework linking the micro-scale notion of statistically stored and geometrically necessary dislocations to the mesoscale notion of plastic strain and strain gradients, a mechanism-based theory of strain gradients (MSG) has been proposed recently (Gao et al., 1998; Huang et al., 1998). In the present work, the strain gradient theory is applied to obtain a more precise understanding of the stress state and crack growth behavior near an interface. The main conclusions and contributions of this research are as follows:

- A perturbation solution of the stress jump over the interface in a bimaterial system has been derived based on the mechanism based strain gradient theory (Gao et al., 1998; Huang et al., 1998). The solution indicates that a high stress triaxiality takes place on the softer material side whereas on the harder material side the strain gradient is higher. The relationships between the length scales, mismatch degree, and the stress and strain gradient are given.
- To investigate the link between the high stress triaxiality and the onset of the subsequent ductile crack growth, a ductile damage model has been used in numerical analysis. A procedure to simulate interface crack growth and the corresponding fracture toughness is introduced and several examples are illustrated. The numerical results are consistent with the theoretical results from the perturbation solution.
- From these investigations, it is our contention that the major effect of the material mismatch in yield capacity is to introduce a high stress triaxiality in the vicinity of the interface. This high stress triaxiality promotes the evolution of damage

Contributed by the Materials Division for publication in the JOURNAL OF ENGINEERING MATERIALS AND TECHNOLOGY. Manuscript received by the Materials Division February 8, 1999; revised manuscript received May 7, 1999. Guest Editors: Assimina A. Pelegri, Ann M. Sastry, and Robert Wetherhold.

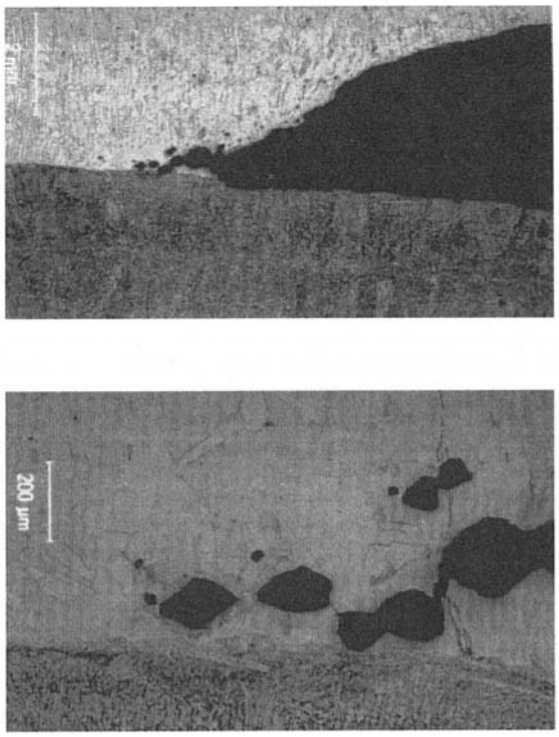

Fig. 1 Damage evolution and ductile crack growth along the interface

in the form of void nucleation, growth and coalescence and results in crack growth along the interface.

2 Applying Gradient Plasticity to Interface Mechanics

2.1 Strain Gradient Plasticity. The strain gradient theory as well as MSG have been developed to consider the effects of length scale when a non-uniform strain exists. In the present work, we employ the notation introduced in (Gao et al., 1998).

We define the strain ϵ_{ij} and the strain gradient η_{ijk} as:

$$\epsilon_{ij} = \tfrac{1}{2}(u_{i,j} + u_{j,i}); \quad \eta_{ijk} = u_{k,ij} \tag{2.1}$$

where the subscript "$_{,i}$" denotes the differential operation with respect to the ith coordinate.

The flow stress $\bar{\sigma}$, after incorporating the strain gradient effect, is:

$$\bar{\sigma} = \sigma_Y[f^2(\bar{\epsilon}) + l\bar{\eta}]^{1/2} \tag{2.2}$$

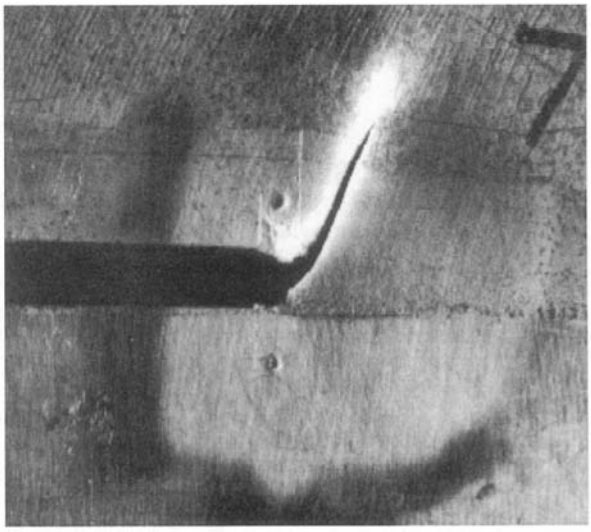

Fig. 2 Crack grows away from the interface

where $\bar{\epsilon}$, $\bar{\eta}$ are the effective strain and effective strain gradient, respectively:

$$\bar{\epsilon} = [\tfrac{2}{3}\epsilon_{ij}\epsilon_{ij}]^{1/2}; \quad \bar{\eta} = \tfrac{1}{2}[\eta_{ijk}\eta_{ijk}]^{1/2} \tag{2.3}$$

The characteristic material length l is given by

$$l = 3\left[\frac{\alpha\mu}{\sigma_Y}\right]^2 b \tag{2.4}$$

where μ, σ_Y, and b denote in turn Young's modulus, yield strength, and Burgers' vector; α is a constant calibrated from experiments. The constitutive equations established in MSG (Gao et al., 1998; Huang et al., 1998) are

$$\sigma'_{ij} = \frac{2\epsilon_{ij}}{3\bar{\epsilon}}\bar{\sigma};$$

$$\tau'_{ijk} = l_\epsilon^2\left[\frac{\bar{\sigma}}{\bar{\epsilon}}(\Gamma_{ijk} - \Pi_{ijk}) + \frac{\sigma_Y^2 f(\bar{\epsilon})f'(\bar{\epsilon})}{\bar{\sigma}}\Pi_{ijk}\right] \tag{2.5}$$

where Γ and Π are functions of ϵ_{ij} and η_{ijk}. For details see (Gao et al., 1998). Here the deviatoric stress tensor and the deviatoric coupling stress tensor, are given by:

$$\sigma'_{ij} = \sigma_{ij} - \tfrac{1}{3}\delta_{ij}\sigma_{kk}, \quad \tau'_{ijk} = \tau_{ijk} - \tfrac{1}{4}(\delta_{ik}\tau_{jpp} + \delta_{jk}\tau_{ipp}) \tag{2.6}$$

Nomenclature

a = the half length of the crack in CCP, or the total length in SE and SPB

b = the scale of Burger's tensor

d = diameter of the domain for RKPM reproducing integration

f_0, f_c, f_e, K_c = volume fraction of initial voids, at coalescence and for nucleation

n_i = component of the unit vector normal to a solid surface

$\hat{t}_i$, $\hat{r}_i$ = normal stress attraction and double stress attraction on a surface

CCP, SE, TPB = central cracked panel, single edged panel, and three point bend specimen

K_c = the accelerate rate of voids volume fraction

J, $J_{\text{far-field}}$ = J-integral and J-integral computed from the far field

W = specimen width

α, β = material constants calibrated from experiments

ϵ_{ij}, η_{ijk} = strain tensor, strain gradient tensor

$\bar{\epsilon}$, $\bar{\eta}$ = effective strain, effective strain gradient

$\dot{\lambda}$ = flow factor

μ, ν = Young's modulu, Possion ratio

$\bar{\sigma}$, σ_Y = flow stress, yield stress

σ_{ij}, σ'_{ij}, H = stress tensor, deviatoric stress tensor, combined hydrostatic stress

σ_m = mean stress

τ_{ijk}, τ'_{ijk} = coupling stress and deviatoric coupling stress tensor

Φ = plastic potential

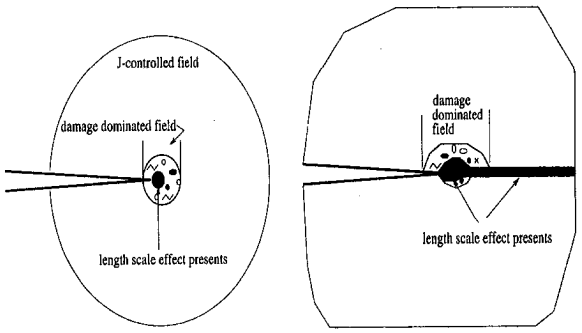

Fig. 3 An illustration of the domain where the effect of length scale may present

and l_ϵ is the mesoscale cell size, defined by

$$l_\epsilon = \beta \frac{\mu}{\sigma_Y} b \tag{2.7}$$

where β is a constant calibrated from experiments.

In the case that the length scale parameters l and l_ϵ are zero, the second relation in Eq. (2.5) vanishes and the first one degenerates to the relationship for classical small strain deformation plasticity. For a monotonic loading process, it coincides with classical incremental plasticity.

For an incompressible solid, the stress tractions $\hat{t}_k$ on the surface of a solid body are

$$\hat{t}_k = Hn_k + n_i(\sigma'_{ik} - \tau'_{ijkj}) + D_k(n_i n_j n_p \tau'_{ijp}) - D_j(n_i \tau'_{ijk}) + (n_i n_j \tau'_{ijk} - n_k n_i n_j n_p \tau'_{ijp})(D_q n_q) \tag{2.8a}$$

where n_i is the unit normal to the surface, H and D_j are the combined measure of the hydrostatic stress and the surface-gradient operator, respectively:

$$H = \tfrac{1}{3}\sigma_{kk} - \tfrac{1}{2}\tau_{jkk,j}, \quad D_j = (\delta_{jk} - n_j n_k)\frac{\partial}{\partial x_k} \tag{2.8b}$$

The double-stress tractions $\hat{r}_k$ tangential to the surface are

$$\hat{r}_k = n_i n_j \tau'_{ijk} - n_k n_i n_j n_p \tau'_{ijp} \tag{2.9}$$

2.2 A Perturbation Solution of the Stress Discontinuity Over an Interface. The bimaterial system to be studied is shown in Fig. 4. A plane strain condition is assumed. In the following analysis the superscript '*I*' and '*II*' are used to denote the quantities in materials *I* and *II*, respectively. We assume that both materials are incompressible and no strain hardening exists, i.e. the perfectly plastic law, therefore for both materials the function $f(\bar{\epsilon})$ Eq. (2.2) becomes:

$$f(\bar{\epsilon}) \equiv 1 \tag{2.10}$$

However, we allow the other mechanical properties and the length scale to differ between the two materials.

On the interface shown in Fig. 4, $n_1 = 0$ and $n_2 = 1$; thus the tangential stress traction $\hat{t}_1$ and the normal stress traction $\hat{t}_2$, defined by Eq. (2.1), are

$$\hat{t}_1 = \sigma'_{21} - 2\tau'_{211,1} - \tau'_{221,2} + \tau'_{222,1},$$

$$\hat{t}_2 = H + \sigma'_{22} - 2\tau'_{212,1} - \tau'_{222,2} \tag{2.11}$$

and the double-stress tractions $\hat{r}_i$ are

$$\hat{r}_1 = \tau'_{221}, \quad \hat{r}_2 = 0 \tag{2.12}$$

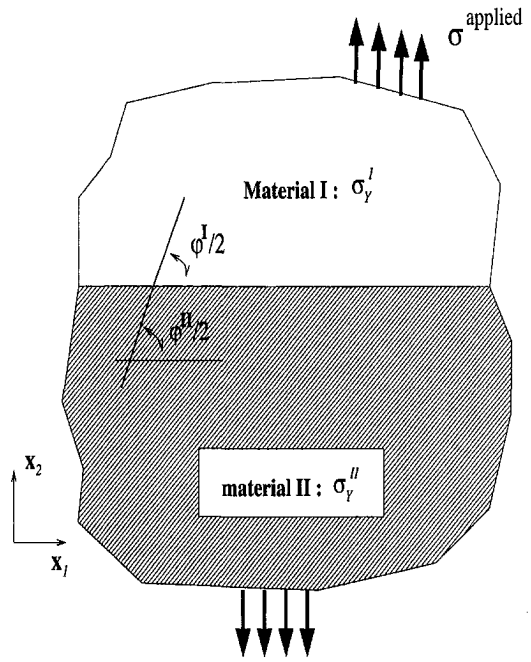

Fig. 4 Schematic of a bimaterial system

The continuity conditions between material "*I*" and "*II*" require:

$$\hat{t}_1^I = \hat{t}_1^{II}, \quad \hat{t}_2^I = \hat{t}_2^{II} \tag{2.13}$$

and

$$\hat{r}_1^I = \hat{r}_1^{II}, \quad \hat{r}_2^I = \hat{r}_2^{II}; \quad \epsilon_{11}^I = \epsilon_{11}^{II}, \quad \eta_{111}^I = \eta_{111}^{II} \tag{2.14}$$

Starting from these conditions, in this section we will establish an asymptotic solution of the stress field around the interface illustrated in Fig. 4 for the bimaterial system obeying Eqs. (2.2) and (2.5).

From the constitutive relationships of MSG given in the previous section one can find that the smallest material constant involved in those equations is "b," the length of Burger's vector. Therefore, in the region close to the interface we assume that all stress components can be expanded in a perturbation series in terms of b, while all strain and strain gradient components are treated as unknown variables. Then by applying the continuity conditions (Eqs. (2.13) and (2.14)) the coefficients of the perturbation series can be determined, so the jump in stress and the strain gradient can be established. In the following analysis only the main results are given.

For both materials, the perturbation expressions of the flow stress $\bar{\sigma}$, combined hydrostatic stress H, deviatoric stress σ'_{ij} and deviatoric coupling stress τ'_{ijk} have the following forms (where $K = I$ or II refers to material I or II, respectively):

$$\sigma^K = \sigma_Y^K(1 + \tfrac{1}{2}\eta^K\omega^K b^I - \tfrac{1}{6}(\eta^K)^2(\omega^K)^2(b^I)^2 + \ldots) \tag{2.15}$$

$$\sigma'^K_{ij} = \sigma'^K_{(0)ij} + \sigma'^K_{(1)ij}\kappa^K b^I + \sigma'^K_{(2)ij}(\kappa^K b^I)^2 + \ldots \tag{2.16}$$

$$H^K = H^K_{(0)} + H^K_{(1)}\kappa^K b^I + H^K_{(2)}(\kappa^K b^I)^2 + \ldots, \tag{2.17}$$

$$\tau'^K_{ij} = \tau'^K_{(0)ij}(\kappa^K b^I)^2 + \tau'^K_{(1)ij}(\kappa^K b^I)^3 + \ldots \tag{2.18}$$

where

$$\omega^K = \kappa^K \frac{l^K}{b^I} = 3\kappa^K\left(\frac{\alpha^K\mu^K}{\sigma_Y^K}\right)^2; \quad \kappa^I = 1, \quad \kappa^{II} = \frac{b^{II}}{b^I} \tag{2.19}$$

For both materials, i.e., $K = I, II$, by substituting Eqs. (2.15 to 2.19) into Eqs. (2.13) and (2.14) one can find that:

$$\hat{t}_1^K = \frac{2\epsilon_{21}^K}{3\bar{\epsilon}^K}\sigma_Y^K + \frac{\epsilon_{21}^K}{3\bar{\epsilon}^K}\sigma_Y^K\eta^K\omega^K b^I + O((b^K)^2) \quad (2.20)$$

$$\hat{t}_2^K = H_0^K + \frac{2\epsilon_{22}^K}{3\bar{\epsilon}^K}\sigma_Y^K + \left(H_1^K\kappa^K + \frac{\epsilon_{22}^K}{3\bar{\epsilon}^K}\sigma_Y^K\eta^K\omega^K\right)b^K + O((b^K)^2) \quad (2.21)$$

and

$$\hat{r}_1^K \simeq O((b^K)^2), \quad \hat{r}_2^K \simeq O((b^K)^2) \quad (2.22)$$

Comparing the first term in Eqs. (2.20) and (2.21) for $K = I$ with that for $K = II$, we get the zeroth order continuity condition by:

$$\frac{\epsilon_{21}^I}{\bar{\epsilon}^I}\sigma_Y^I = \frac{\epsilon_{21}^{II}}{\bar{\epsilon}^{II}}\sigma_Y^{II}, \quad H_{(0)}^I + \frac{2\epsilon_{22}^I}{3\bar{\epsilon}^I}\sigma_Y^I = H_{(0)}^{II} + \frac{2\epsilon_{22}^{II}}{3\bar{\epsilon}^{II}}\sigma_Y^{II} \quad (2.23)$$

A statically determinant solution that satisfies this condition can be written as

$$\frac{2\epsilon_{21}^K}{\bar{\epsilon}^K\sqrt{3}} = \cos\varphi^K, \quad \frac{2\epsilon_{22}^K}{\bar{\epsilon}^K\sqrt{3}} = \sin\varphi^K; \quad \text{where } K = I, II \quad (2.24)$$

This solution describes a slip-line field around the interface which can be derived directly from the characteristic field theory in classical plasticity (Hill, 1963), since in the zeroth order governing equation (2.24) there is no length scale present. The definitions of the angle φ^I and φ^{II} are illustrated in Fig. 4.

From Eq. (2.24) one can find when $\varphi^I = \varphi^{II} = -(\pi/2)$ the zeroth order continuity condition (2.23) can be satisfied exactly. The corresponding zeroth order hydrostatic stress jump over the interface is

$$H_{(0)}^I - H_{(0)}^{II} = \frac{\sigma_Y^{II} - \sigma_Y^I}{\sqrt{3}} \quad (2.25)$$

By comparing the first order term for $K = I$ in Eqs. (2.20) and (2.21) with that of $K = II$, respectively, and omitting some intermediate steps, we can express the jump in strain gradient over the interface from the first order solution of the continuity condition of $\hat{t}_1$ direction:

$$\frac{\eta^I}{\eta^{II}} = \frac{(\mu^{II}\sigma^I)^2}{(\mu^I\sigma^{II})^2} \quad (2.26)$$

Similarly, from the solution of $\hat{t}_2$:

$$\kappa^I H_1^I - \kappa^{II}H_1^{II} = 2(\kappa^I H_0^I - \kappa^{II}H_0^{II})\eta^{II}\omega^{II} \quad (2.27)$$

the first order solution for the jump of the combined hydrostatic stress.

Leaving out terms higher than $O(b^I)$ and assuming $\kappa^I = \kappa^{II} = 1$ in Eq. (2.19) we determine the jump in hydrostatic stress over the interface:

$$\frac{H^I - H^{II}}{\sigma_Y^{II}} = (1 + 2\eta^I l^I)\left(\frac{1}{\sqrt{3}} - \sigma_Y^I\sigma_Y^{II}\sqrt{3}\right) \quad (2.28)$$

Assuming that $\alpha^I = \alpha^{II}$ and $\kappa^{II} = 1$, from Eq. (2.26) the relationship between the ratio η^I/η^{II} and σ_Y^{II}/σ_Y^I, the mismatch degree in yield strength, are displayed in Fig. 5 where assuming the material I is softer than the material II. From this diagram one observes that the strain gradient at the harder material side, i.e., η^{II}, is lower than that at the softer material side, especially when the ratio μ^{II}/μ^I is large. However, by increasing the ratio σ_Y^{II}/σ_Y^I this difference will be reduced. This effect can be explained by considering that the higher yield strength material contains the deformation caused by the material discontinuity in smaller relatively area near the interface as compared to that of the softer material.

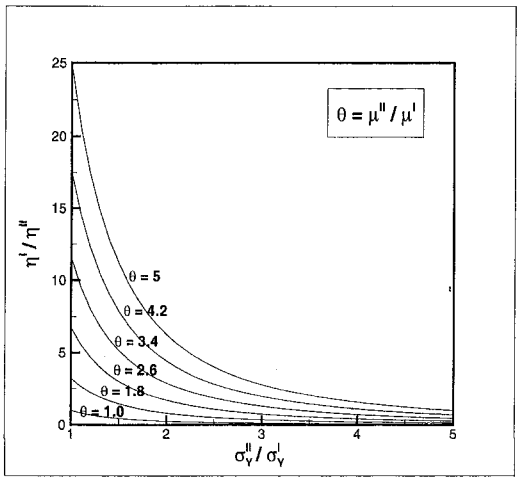

Fig. 5 The discontinuity of strain gradient over an interface

From Eq. (2.28), the discontinuity in the combined hydrostatic stress versus the mismatch degree in yield strength are displayed in Fig. 6. In contrast to the discontinuity in strain gradient, one finds that a higher hydrostatic stress always takes place always on the softer material side.

The hydrostatic stress can be interpreted as the stress triaxiality at a material point. A qualitative explanation of the elevation of the stress triaxiality is illustrated in Fig. 7. Assuming the bimaterial panel is under purely homogeneous uniaxial tension, the elongation and, hence, the transverse reduction of area would be higher in the softer material since it yields at an earlier stage. However, the corresponding velocity field is not admissible. The continuity condition of deformation requires additional transverse stress near the interface. These transverse stresses are tensile and increase the hydrostatic stress in the softer material, while compressive and reduce the hydrostatic stress in the high strength material.

2.3 The Asymptotic Stress-Strain Field at an Interface Crack Tip. The analysis in the previous section shows that the slip line solution can be used as the zeroth order approximation of the solution with strain gradient theory. In this subsection, several slip line solutions of an interface crack problem are briefly introduced.

A review of the interface crack tip field analysis has been given in the first section. Here the asymptotic solutions for a crack tip at the interface between dissimilar perfectly-plastic materials will be discussed. The bimaterial system is mismatched in yield strength.

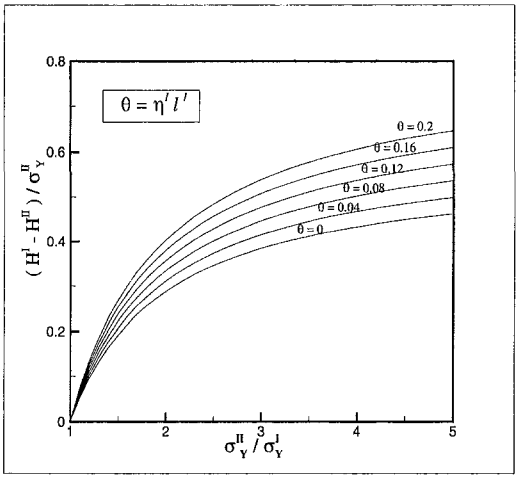

Fig. 6 The discontinuity of stress triaxiality versus mismatch degree over an interface

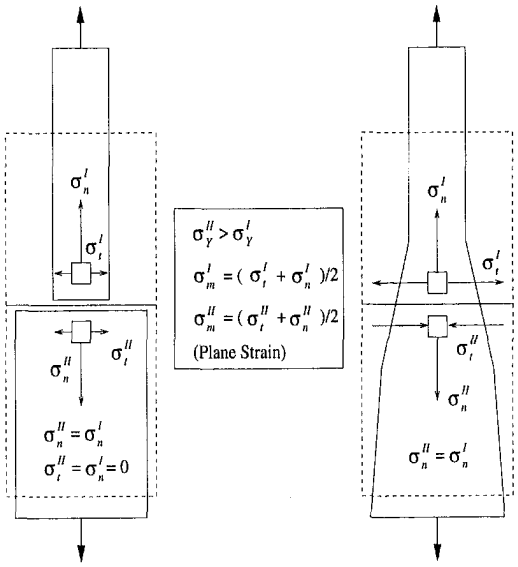

Fig. 7 A qualitative explanation of the discontinuity of stress triaxiality over an interface

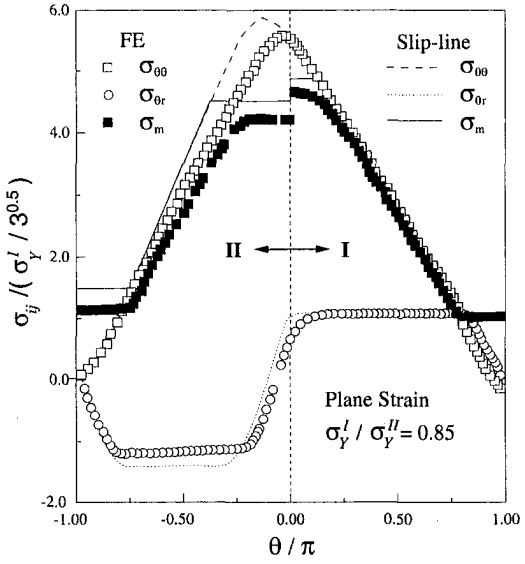

Fig. 9 Stress distributions around the interface crack tip; slip-line and FE solution

For a sharp crack tip the slip-line solution has been constructed as shown in Fig. 8, where material *I* is softer than material *II*, i.e., $\sigma_Y^{II} > \sigma_Y^I$ and perfect bonding is assumed.

At the horizontal line ahead of the crack tip, the conclusion drawn from Eq. (2.28) is also available, i.e. in the softer material the stress triaxiality is higher than in the harder material. From the zeroth order continuity condition over interface (Eq. (2.25)) one can conclude that when σ_Y^I/σ_Y^{II} is less than about 0.7, the harder material remains in the elastic regime. Another conclusion from the slip-line solution is: in the harder material the maximum hoop stress does not occur just ahead the crack tip, but away from the interface, as shown in Fig. 9. For comparison, a finite element solution is also displayed in this diagram. Both finite element and slip-line solution yield the same conclusion.

The slip-line field in Fig. 8 is derived assuming no blunting at the crack tip. Assuming the profile of a blunted crack tip is semi-similar during deformation, a slip-line field has been constructed as shown in Fig. 10. It is contained by the solution in Fig. 8 where the constant stress regions A and C in the softer material side remain, the fan region B focuses intense strain into the region "**abcd**" directly ahead of the blunted tip. A kinematic field has also been constructed along the slip lines $\widehat{ac}$ and $\widehat{bc}$. A maximum shear strain may take place at the point C. On the other hand, in the region "**acd**" plastic deformations are constrained by the harder phase below the interface which induces a high stress triaxiality. The maximum stresses appear at the point "**d**." If $\sigma_Y^I/\sigma_Y^{II} < 0.707$ we obtain the stresses at this point from the slip-line solution:

$$\sigma_{11} = \sigma_{22} = \sigma_m = \frac{\sigma_Y^I}{\sqrt{3}}\left(1 + \frac{3\pi}{2}\right) \tag{2.29}$$

2.4 Linking of the Theoretical Analysis to Ductile Damage Induced Crack Growth. Ductile fracture is the accumulation process of damage in the form of voids. The nucleation, growth and coalescence of micro-voids are mainly governed by the intensity of stress triaxiality (Rice and Tracey, 1969). The solutions derived in the previous two subsections (Eqs. 2.28 and 2.29) reveal that a high stress triaxiality exists at the softer phase side. In addition, the quantitative relationship between strain gradient, material mismatch, and the elevation of stress triaxiality is given. There is no doubt that this elevated stress triaxiality has strong effects on the fracture toughness for a bimaterial system.

Considering an elastic-plastic material element without damage, it enters a state of yield when

$$\bar{\sigma} - \sigma_Y = 0 \tag{2.30}$$

If ductile damage exists at scales coarser than that of the strain gradient theory concerned, the yield condition for the material element can be written generally in the form as follows (Hao et al., 1999):

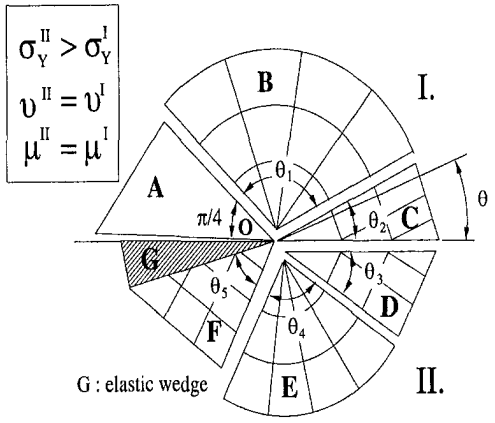

Fig. 8 An asymptotic crack tip slip-line field

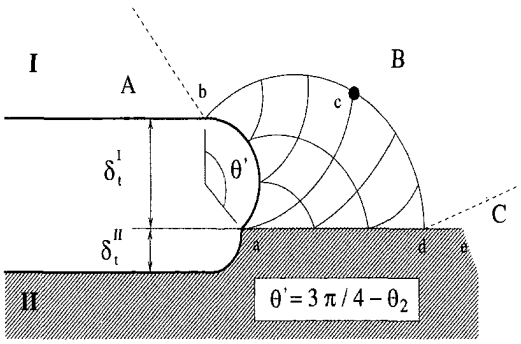

Fig. 10 An asymptotic slip-line field around a blunted interface crack tip

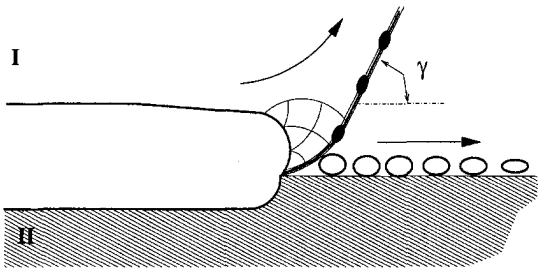

Fig. 11 An illustration of the two possible crack growth paths, where γ ranges from $\pi/4$ to $\pi/2$

$$\Phi\left(\frac{\bar{\sigma}}{\sigma_Y}, \frac{\sigma_m}{\sigma_Y}, f\right) = \left(\frac{\bar{\sigma}}{\sigma_Y}\right)^2 + \left(1 + \frac{1}{m_{20}}\right) f m_1 \exp\left(\frac{3\sigma_m}{2\sigma_Y}\right) - 1 = 0 \quad (2.31)$$

where we use σ_m to represent the stress triaxiality. From this relation one observes that if the volume fraction of voids: f, is nonzero, the material element yields by increasing either the equivalent stress $\bar{\sigma}$ or the stress triaxiality. The yield surface is determined by the combination of the material yield stress σ_Y and the damage f. When f reaches its critical value, the yield shrink to the original point, i.e., $\bar{\sigma} = 0$, $\sigma_m = 0$. It refers to the fully collapsed state and a damage induced cracking takes place at this material element.

Thus, a damage induced crack occurs easily along an interface in the softer material, since the previous analysis indicates an elevated stress triaxiality exists on that side. This explains the experimental result presented in Fig. 1. However, Eq. (2.31) hints that yielding depends also upon $\bar{\sigma}$ which is directly related to the shear stress and strain. The slip-line field solution in Fig. 10 predicts a kinematic displacement field which can be activated along shear bands when the global boundary conditions do not provide enough constraint. Under this situation, the crack will grow following the localized large strain along the shear band, and subsequently away from the interface, as illustrated in Fig. 11. This conclusion coincides with the observation shown in Fig. 2 of which tearing dominates and crack grows along the shear band.

3 Numerical Procedures and Crack Growth Simulation

In this section numerical simulations are performed to demonstrate the effects of crack growth path on fracture toughness quantitatively and to verify the conclusions obtained in the previous section.

3.1 Numerical Procedures. To simulate ductile crack growth, the plastic potential from Eq. (2.31) and the damage evolution law introduced in (Chu and Needleman, 1980; Needleman and Tvergaard, 1987) have been applied to establish the constitutive relationship.

The finite element method and meshless method (Belytschko et al., 1994; Liu et al., 1996; Liu et al., 1995; Liu et al., 1995; Liu and Chen, 1995; Liu et al., 1998; Liu et al., 1996) are employed in the numerical simulations. In the finite element simulation, to avoid the volumetric locking due to the additional constraint caused by material mismatching, the multiple quadrature under-integrated element (W. K. Liu, 1985; Liu et al., 1994; Liu et al., 1997), an element free from shear and volume locking and with hourglass control, has been used in the finite element analysis. The implementation of the constitutive law with damage into finite element and RKPM (Reproducing Kernel Particle Method) is introduced in (Hao et al., 1999). For a discussion of meshless methods, readers are urged to consult (Belytschko et al., 1994; Jun et al., 1998; Liu and Jun, 1998; Liu et al., 1997; Chen et al., 1996) and references cited therein.

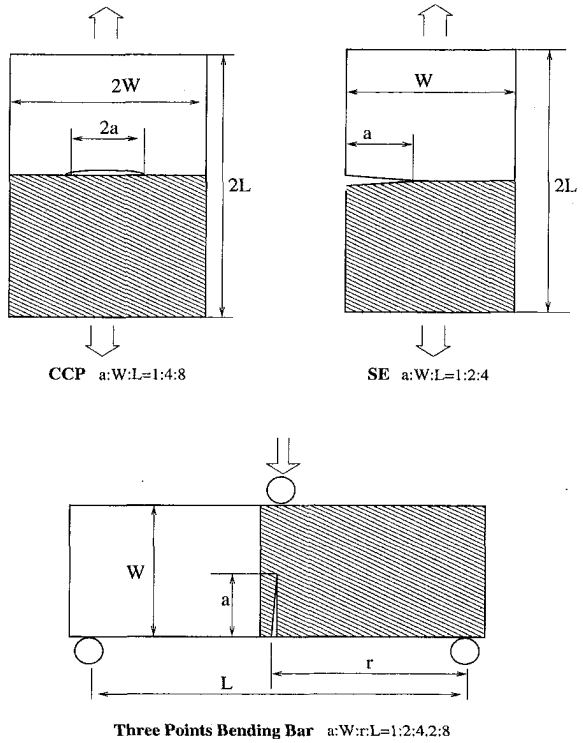

Fig. 12 The two types of specimens analyzed

3.2 The Specimen Analyzed. The Central Cracked Panel (CCP) and the Singer Edge panel (SE) under tension and the notched three point bending specimen have been analyzed, see Fig. 12. The stress-strain curve of a uniaxial tension specimen made of 20MoMnNiB mild steel has been used in the computation. The mechanical properties are listed in Table 1, where n denotes the strain hardening exponent. Several mismatch specimens with varying yield strength in the harder phase have been computed. The values of the ratio $M_Y(=\sigma_Y^I/\sigma_Y^{II})$ are given in the examples demonstrated following.

The yield condition from Eq. (2.31) has been used in the numerical simulation. The damage parameters calibrated in (Hao et al., 1999) have been used, see Table 2.

3.3 Numerical Simulation and Discussion. In this section results from performed simulations under various conditions are discussed.

Figure 13 shows the simulated fracture toughness (J-R curve) for the bimaterial CCP specimens in which a crack is located in the softer material and parallel to the interface. The J-integral is computed from the global energy release rate of the specimen. A distance between the crack tip and the interface may exist which is denoted by "ξ." Comparing the computed J-R curve for the case

Table 1 Mechanical properties

μ (MPa)	ν	σ_Y (MPa)	n
21000	0.3	490	≈0.21

Table 2 Damage parameters

f_0	f_c	K_c	f_n
0.0001	0.03	3	0.004

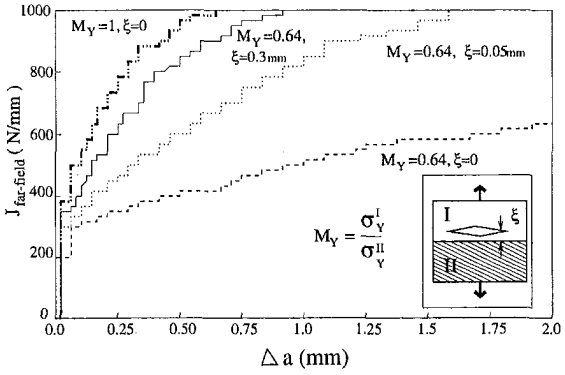

Fig. 13 Simulated J-R curves for varying values of ξ

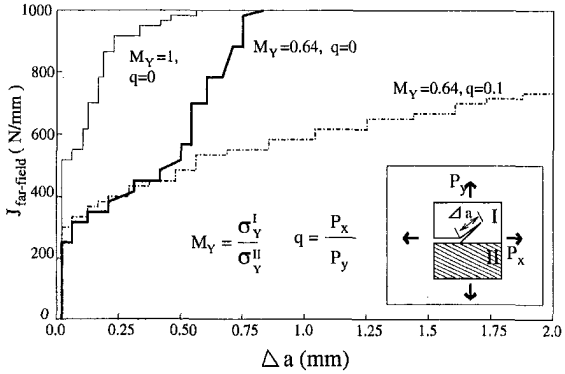

Fig. 15 Simulated J-R curves for varying amounts of transverse constraint

when a crack is just on the interface ($\xi = 0$), a significant increase of the fracture toughness can be seen when a crack is a small distance away from the interface. Obviously, the high strain gradient and the stress triaxiality due to material heterogeneity are only localized in the immediate vicinity of the interface. When a crack tip

Assuming that a crack is located just at the interface of the subject CCP specimen and then by varying the mismatch degree $[M_Y = (\sigma_Y^I/\sigma_Y^{II})]$, the resulting simulated J-R curves are shown in Fig. 14. A strong reduction in the crack growth resistance can be seen when the mismatch degree in yield strength increases (M_Y decreases). But this tendency of the toughness reduction does not hold after M_Y is less than 0.64. This result coincides with the prediction obtained from the slip-line solution in Fig. 8 which claims that when the ratio $(\sigma_Y^I/\sigma_Y^{II}) < 0.707$ the zeroth solution of the stress distribution in material I becomes independent to M_Y. Meanwhile material II remains in an elastic state. However, it can be expected that the fracture toughness may change significantly when a very ductile material is bonded to another material with a high degree of mismatch, since under this situation the effect of the strain gradient becomes stronger.

Figure 16 shows a simulation of the SE specimen with the contours of equivalent plastic strain, equivalent stress, and damage which represents the induced crack. The crack grows away from the interface as the geometry and load conditions of the SE specimen provide less global constraint than in the CCP. In this case the global kinematically admissible displacement field is activated. Thus, the plastic strain along the shear band dominates the crack tip field and the crack grows via ductile tearing. If one applies a tiny transverse tension (about $\frac{1}{10}$ of the vertical tension) to the specimen, while keeping all other parameters unchanged, the crack grows straight along the interface, as shown in Fig. 17. Adding a transverse tension is identical to increasing the global constraint which will block shear deformation and raise the level of stress triaxiality around the crack tip. This elevated stress triaxiality promotes the evolution of damage in the form of microvoids and ductile crack growth along the interface. The corresponding J-R curves are displayed in Fig. 15. From this diagram one finds that both cases have a similar initial J-integral value, but after some crack growth an obvious increase in the resistance capacity against fracture can be seen for the crack which grows away from the interface and propagates into the softer material. From both Figs. 14 and 15, a significant change of the resistance curve of bimaterial specimens is observed compared to the homogeneous case ($M_Y = 1$).

To investigate the effect of "nonlocal theory" on the numerical simulation, the notched bimaterial three point bending bar has been analyzed using RKPM. The bimaterial system is mismatched in Young's modulus. The crack is located in the harder phase with a specified distance away from the interface. The simulation results are displayed in Fig. 18 with the contours of damage representing the damage induced crack, where d denotes the diameter of the interpolating domain used in the meshless method (Liu et al., 1996; Belytschko et al., 1994). In the case with a smaller d the

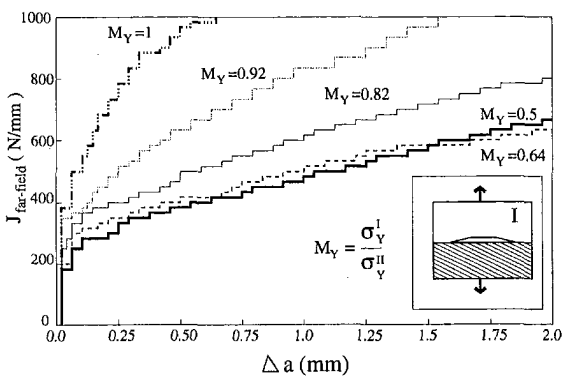

Fig. 14 Simulated J-R curves for varying values of M_Y

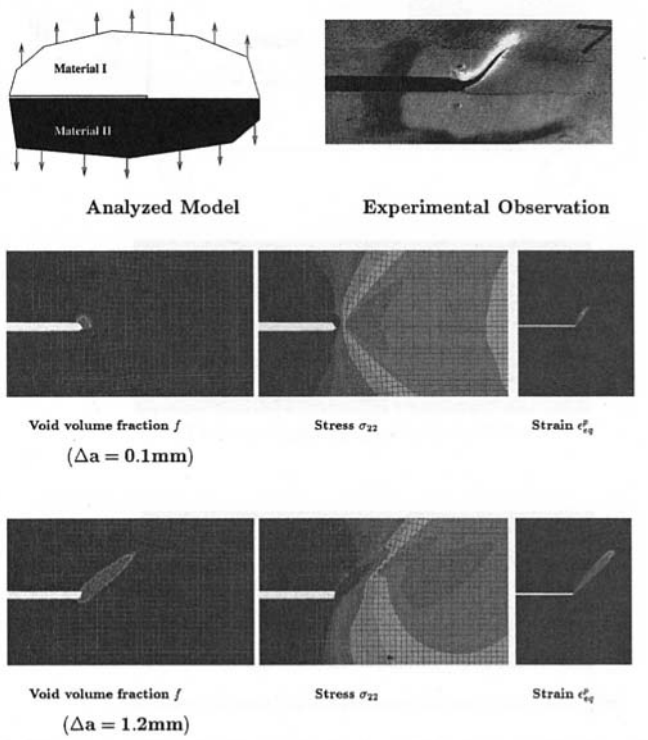

Fig. 16 Computed interface crack growth without transverse constraint

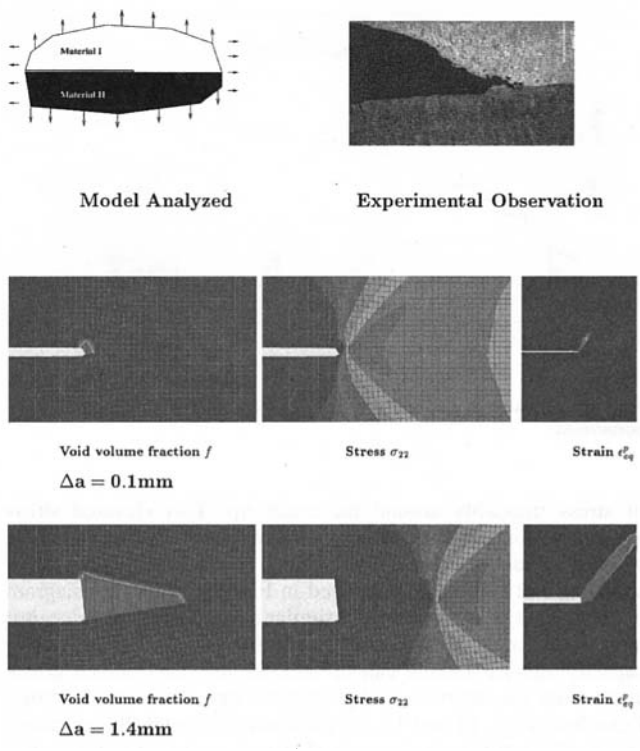

Fig. 17 Computed interface crack growth with transverse constraint

crack keeps growing in the harder material since the imposed boundary conditions induce a mixed mode load on the crack tip which drives the crack growth away from the interface in the harder phase. However, when d is large enough that the domain influence Ω for the nodes near the crack tip may cover some

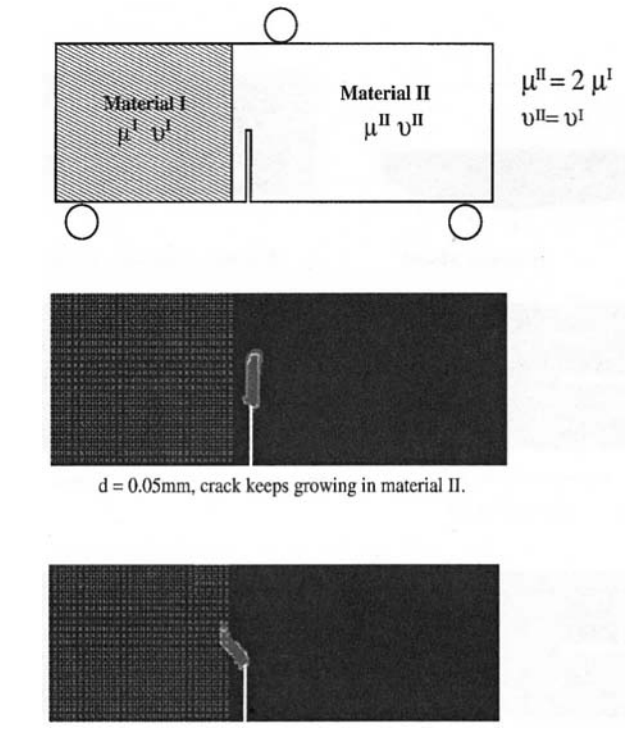

Fig. 18 Effect of the nonlocal smoothing domain size on simulated crack growth

interaction between the two materials and the effect of interface may be included in these nodes, the crack path deviates toward the interface then grows along it.

From the theoretical analysis and numerical simulations we can conclude that an interface crack always tends to grow into the softer phase if no debonding takes place. It may grow along a shear band and deviate into the softer phase; or go straight along the interface. In the latter case a significant decrease in fracture toughness can occur compared to the homogeneous case.

4 Summary

In this paper the interface crack growth problem has been investigated based on the mechanism-based strain gradient plasticity (MSG) and ductile damage theory. A perturbation solution of the stress and strain gradient discontinuities that occur at the interface have been derived. From the solution it is found that for a bimaterial system mismatched in yield capacity an elevated stress triaxiality takes place on the softer material side whereas a raised strain gradient occurs in the harder material. The value of this elevation is determined by the length scale and the degree of mismatch in yield strength. Numerical simulation of damage induced interfacial crack growth has been performed using both finite element and RKPM. The numerical simulation verifies the predictions of the theoretical analysis and matches the experimental observation. The conclusions and results of this study are summarized in the following:

- Two kinds of failure mechanisms exist in ductile crack growth. They are damage induced cracking which is mainly controlled by the stress triaxiality and pure ductile tearing dominated crack growth which is mainly controlled by the shear stress and strain. In a ductile fracture process both mechanisms may exist simultaneously.
- The theoretical analysis indicates: the major effects of material mismatch in yield strength at an interface are to raise the stress triaxiality in the softer phase whereas a higher strain gradient exists in the harder side. This stress triaxiality is proportional to the degree of material mismatch in yield capacity and the product of strain gradient and the length scale.
- Since damage in the form of void nucleation, growth and coalescence are mainly controlled by the level of stress triaxiality, this kind of damage induced crack growth will easily take place along an interface. In this case the bimaterial system has a lower toughness against fracture.
- The slip-line solution predicts a kinematically admissable displacement field around a blunted interface crack tip. If the global constraint in a specimen, provided by the specimen geometry and boundary conditions, is not too high, this kind of displacement field will be activated and the specimen will fully yield. Under this situation ductile tearing dominated crack growth may occur along the predicted slip-line, provided the stress triaxiality is too high or the material is not sensitive to damage.

Acknowledgment

The support of this research by Army Research Office (ARO) and National Science Foundation (NSF) to Northwestern University is gratefully acknowledged.

Sponsored in part by the Army High Performance Computing Research Center (AHPCRC) under the auspices of the Department of the Army Research Laboratory. The content does not necessarily reflect the position or the policy of the government, and no official endorsement should be inferred.

The authors are also grateful to Mr. John Dolbow and Dr. C. T. Chang for many helpful comments and suggestions during the preparation of this manuscript.

References

Belytschko, T., Y. Y. Lu, and L. Gu, 1994, "A new implementation of the element free Galerkin method," *Computer Methods in Applied Mechanics and Engineering,* Vol. 113, pp. 397–414.

Chen, J. S., C. Pan, and W. K. Liu, 1996, "Reproducing kernel particle methods for large deformation analysis of nonlinear structures," *Computer Methods in Applied Mechanics and Engineering,* Vol. 139, pp. 195–228.

Chu, C. C., and A. Needleman, 1980, "Void nucleation effects in biaxially strached sheets," *J. of Engineering Material and Technology,* Vol. 102, pp. 249–256.

Evans, A. G., and B. J. Dalgleish, 1990, "The fracture resistance of metal-ceramic interfaces," *Acta Met. Mater.,* Vol. 40, pp. S295–S306.

Fleck, N. A., and J. W. Hutchinson, 1993, "A phenomenological theory for strain gradient effects in plasticity," *J. of Mechanics and Physics of Solids,* Vol. 41, pp. 1825–1857.

Fleck, N. A., and J. W. Hutchinson, 1997, Strain gradient theory, *Advances in Applied Mechanics,* ed. J. W. Hutchinson and T. Y. Wu, Vol. 33, pp. 295–361.

Gao, H., Y. Huang, W. D. Nix, and J. W. Hutchinson, 1998, "Mechanism-based strain gradient plasticity: I theory," In preparation.

Hao, S., W. Brocks, M. Kocak, and K.-H. Schwalbe, 1996, Simulation of the ductile crack growth on interface (fusion line), *2nd Int. Symp. on Mismatch,* Reinstoff, Germany.

Hao, S., W. K. Liu, and C. T. Chang, 1999, "Computation implementation of damage models by finite element and mechfree methods" (accepted and to be appeared in) *Computer Methods in Applied Mechanics and Engineering.*

Hill, R., 1963, *J. of Mechanics and Physics of Solids,* Vol. 11, p. 357.

Huang, Y., H. Gao, W. D. Nix, and J. W. Hutchinson, 1998, "Mechanism-based strain gradient plasticity: II analysis," In preparation.

Hutchinson, J. W., M. Mear, and J. R. Rice, 1987, "Crack paralleling an interface between dissimilar media," ASME *Journal of Applied Mechanics,* Vol. 54, pp. 828–832.

Jun, S., W. K. Liu, and T. Belytschko, 1998, "Explicit reproducing kernel particle methods for large deformation problems," *International J. for Numerical Methods in Engineering,* Vol. 41, pp. 137–166.

Liu, W. K., and Y. Chen, 1995, "Wavelet and multiple scale reproducing kernel methods," *International J. for Numerical Methods in Fluids,* Vol. 21, pp. 901–931.

Liu, W. K., Y. Chen, C. T. Chang, and T. Belytschko, 1996, "Advances in multiple scale kernel particle methods," A Special Feature Article for the 10th Anniversary Volume of *Computational Mechanics,* Vol. 18(2), pp. 73–111.

Liu, W. K., Y. Chen, R. A. Uras, and C. T. Chang, 1996, "Generalized multiple scale reproducing kernel particle methods," *Computer Methods in Applied Mechanics and Engineering,* Vol. 139, pp. 91–158.

Liu, W. K., Y. Guo, S. Tang, and T. Belytschko, 1997, "A multiple-quadrature eight-node hexahedral finite element for large deformation elastioplastic analysis," *Computer Methods in Applied Mechanics and Engineering,* Vol. 154, (1998), pp. 69–132.

Liu, W. K., W. Hao, Y. Chen, S. Jun, and J. Gosz, 1997, "Multiresolution reproducing kernel particle methods," *Computational Mechanics,* Vol. 20(4), pp. 295–309.

Liu, W. K., Y. K. Hu, and T. Belytschko, 1994, "Multiple quadraturem underintegrated finite elements," *International J. for Numerical Methods for Engineering,* Vol. 37, pp. 3263–3289.

Liu, W. K., and S. Jun, 1998, "Multiple scale reproducing kernel particle methods for large deformation problems," *International J. for Numerical Methods in Engineering,* Vol. 41, pp. 1339–1362.

Liu, W. K., S. Jun, S. Li, J. Adee, and T. Belytschko, 1995, "Reproducing kernel particle methods for structural dynamics," *International J. for Numerical Methods for Engineering,* Vol. 38, pp. 1655–1679.

Liu, W. K., S. Jun, and Y. F. Zhang, 1995, "Reproducing kernel particle methods," *International Journal for Numerical Methods in Fluids,* Vol. 20, pp. 1081–1106.

Liu, W. K., R. A. Uras, and Y. Chen, 1998, "Enrichment of the finite element method with the reproducing kernel particle method," ASME *J. of Applied Mechanics,* Vol. 64, pp. 861–870.

Liu, W. K., A. Uras, J. S. O., 1985, "Finite element stabilization matrices—a unification approach," *Computer Methods in Applied Mechanics and Engineering,* Vol. 53, pp. 13–46.

Needleman, A., and V. Tvergaard, 1987, "An analysis of ductile rupture modes at a crack tip," *J. of Mechanics and Physics of Solids,* Vol. 35, pp. 151–183.

Petrovski, B., and M. Kocak, 1993, "Evaluation of the fracture behaviour of strength mis-matched steel weld joints with surface cracked tensile panels and senb specimens," *Mis-Matching of Weld,* ed., K.-H. Schwalbe and M. Kocak, pp. 511–537.

Reimanis, I. E., e. a., 1990, "Effects of plasticity on the crack propergation resistance of a metal/ceramic interface," *International J. of Fracture,* Vol. 38, pp. 2645–2652.

Rice, J. R., 1988, "Elastic fracture mechanics concepts for interfacial cracks," ASME *J. of Applied Mechanics,* Vol. 55, pp. 418–423.

Rice, J. R., and D. M. Tracey, 1969, "On the ductile enlargement of voids in triaxial stress field," *J. Mech. Phys. Solids,* Vol. 17, pp. 2–15.

Shih, C. F., and R. J. Asaro, 1991, "Elastic-plastic analysis of cracks on bi-material interfaces: Part III—large sacle yielding," ASME *J. of Applied Mechanics,* Vol. 58, pp. 450–463.

Williams, M. L., 1959, "The stresses around a fault or crack in dissimilar media," *Bulletin of the Seismological Society of America,* Vol. 49, pp. 199–204.

Xu, X.-P., and A. Needleman, 1995, "Numerical simulations of dynamic interfacial crack growth allowing for crack growth away from the bond line," *Int. J. of Fracture,* Vol. 74, pp. 253–275.

Zywicz, E., and D. M. Parks, 1992, "Small-scale yielding interfacial crack tip fields," *J. Mech. Phys. Solids,* Vol. 40, pp. 511–536.